Search for WIMP Inelastic Scattering off Xenon Nuclei with XENON100

Aprile, E.; Aalbers, J.; Breur, P.A.; Brown, A.; Colijn, A.P.; Decowski, M.P.; Tiseni, A.; XENON Collaboration

DOI
10.1103/PhysRevD.96.022008

Publication date
2017

Document Version
Final published version

Published in
Physical Review D. Particles and Fields

Citation for published version (APA):
Aprile, E., Aalbers, J., Breur, P. A., Brown, A., Colijn, A. P., Decowski, M. P., Tiseni, A., & XENON Collaboration (2017). Search for WIMP Inelastic Scattering off Xenon Nuclei with XENON100. *Physical Review D. Particles and Fields*, *96*(2), [022008]. https://doi.org/10.1103/PhysRevD.96.022008

PHYSICAL REVIEW D **96,** 022008 (2017)

Search for WIMP inelastic scattering off xenon nuclei with XENON100

E. Aprile,[1] J. Aalbers,[2] F. Agostini,[3,4] M. Alfonsi,[5] F. D. Amaro,[6] M. Anthony,[1] F. Arneodo,[7] P. Barrow,[8] L. Baudis,[8,*] B. Bauermeister,[9] M. L. Benabderrahmane,[7] T. Berger,[10] P. A. Breur,[2] A. Brown,[2] E. Brown,[10] S. Bruenner,[11] G. Bruno,[3] R. Budnik,[12] L. Bütikofer,[13,†] J. Calvén,[9] J. M. R. Cardoso,[6] M. Cervantes,[14] D. Cichon,[11] D. Coderre,[13,†] A. P. Colijn,[2] J. Conrad,[9] J. P. Cussonneau,[15] M. P. Decowski,[2] P. de Perio,[1] P. Di Gangi,[4] A. Di Giovanni,[7] S. Diglio,[15] G. Eurin,[11] J. Fei,[16] A. D. Ferella,[9] A. Fieguth,[17] W. Fulgione,[3,18] A. Gallo Rosso,[3] M. Galloway,[8] F. Gao,[1] M. Garbini,[4] C. Geis,[5] L. W. Goetzke,[1] Z. Greene,[1] C. Grignon,[5] C. Hasterok,[11] E. Hogenbirk,[2] R. Itay,[12] B. Kaminsky,[13,†] S. Kazama,[8] G. Kessler,[8] A. Kish,[8] H. Landsman,[12] R. F. Lang,[14] D. Lellouch,[12] L. Levinson,[12] Q. Lin,[1] S. Lindemann,[11,13] M. Lindner,[11] F. Lombardi,[16] J. A. M. Lopes,[6,‡] A. Manfredini,[12,§] I. Maris,[7] T. Marrodán Undagoitia,[11] J. Masbou,[15] F. V. Massoli,[4] D. Masson,[14] D. Mayani,[8] M. Messina,[1] K. Micheneau,[15] A. Molinario,[3] K. Mora,[9] M. Murra,[17] J. Naganoma,[19] K. Ni,[16] U. Oberlack,[5] P. Pakarha,[8] B. Pelssers,[9] R. Persiani,[15] F. Piastra,[8] J. Pienaar,[14] V. Pizzella,[11] M.-C. Piro,[10] G. Plante,[1] N. Priel,[12] L. Rauch,[11] S. Reichard,[14] C. Reuter,[14] A. Rizzo,[1] S. Rosendahl,[17] N. Rupp,[11] J. M. F. dos Santos,[6] G. Sartorelli,[4] M. Scheibelhut,[5] S. Schindler,[5] J. Schreiner,[11] M. Schumann,[13] L. Scotto Lavina,[20] M. Selvi,[4] P. Shagin,[19] M. Silva,[6] H. Simgen,[11] M. v. Sivers,[13,†] A. Stein,[21] D. Thers,[15] A. Tiseni,[2] G. Trinchero,[18] C. Tunnell,[2,22] M. Vargas,[17] H. Wang,[21] Z. Wang,[3] Y. Wei,[8] C. Weinheimer,[17] J. Wulf,[8] J. Ye,[16] and Y. Zhang[1]

(XENON Collaboration)[‖]

[1]*Physics Department, Columbia University, New York, New York 10027, USA*
[2]*Nikhef and the University of Amsterdam, Science Park, 1098XG Amsterdam, Netherlands*
[3]*INFN-Laboratori Nazionali del Gran Sasso and Gran Sasso Science Institute, 67100 L'Aquila, Italy*
[4]*Department of Physics and Astrophysics, University of Bologna and INFN-Bologna, 40126 Bologna, Italy*
[5]*Institut für Physik & Exzellenzcluster PRISMA, Johannes Gutenberg-Universität Mainz, 55099 Mainz, Germany*
[6]*LIBPhys, Department of Physics, University of Coimbra, 3004-516 Coimbra, Portugal*
[7]*New York University Abu Dhabi, 129188 Abu Dhabi, United Arab Emirates*
[8]*Physik-Institut, University of Zurich, 8057 Zurich, Switzerland*
[9]*Oskar Klein Centre, Department of Physics, Stockholm University, AlbaNova, Stockholm SE-10691, Sweden*
[10]*Department of Physics, Applied Physics and Astronomy, Rensselaer Polytechnic Institute, Troy, New York 12180, USA*
[11]*Max-Planck-Institut für Kernphysik, 69117 Heidelberg, Germany*
[12]*Department of Particle Physics and Astrophysics, Weizmann Institute of Science, Rehovot 7610001, Israel*
[13]*Physikalisches Institut, Universität Freiburg, 79104 Freiburg, Germany*
[14]*Department of Physics and Astronomy, Purdue University, West Lafayette, Indiana 47907, USA*
[15]*SUBATECH, IMT Atlantique, CNRS/IN2P3, Université de Nantes, Nantes 44307, France*
[16]*Department of Physics, University of California, San Diego, California 92093, USA*
[17]*Institut für Kernphysik, Westfälische Wilhelms-Universität Münster, 48149 Münster, Germany*
[18]*INFN-Torino and Osservatorio Astrofisico di Torino, 10125 Torino, Italy*
[19]*Department of Physics and Astronomy, Rice University, Houston, Texas 77005, USA*
[20]*LPNHE, Universit Pierre et Marie Curie, Universit Paris Diderot, CNRS/IN2P3, Paris 75252, France*
[21]*Physics & Astronomy Department, University of California, Los Angeles, California 90095, USA*
[22]*Department of Physics & Kavli Institute of Cosmological Physics, University of Chicago, Chicago, Illinois 60637, USA*

(Received 18 May 2017; published 25 July 2017)

We present the first constraints on the spin-dependent, inelastic scattering cross section of weakly interacting massive particles (WIMPs) on nucleons from XENON100 data with an exposure of 7.64×10^3 kg · days. XENON100 is a dual-phase xenon time projection chamber with 62 kg of active mass, operated at the Laboratori Nazionali del Gran Sasso (LNGS) in Italy and designed to search for nuclear

---

[*] laura.baudis@uzh.ch

[†] Also at Albert Einstein Center for Fundamental Physics, University of Bern, Bern, Switzerland.

[‡] Also at Coimbra Engineering Institute, Coimbra, Portugal.

[§] alessandro.manfredini@weizmann.ac.il

[‖] xenon@lngs.infn.it

2470-0010/2017/96(2)/022008(8)

recoils from WIMP-nucleus interactions. Here we explore inelastic scattering, where a transition to a low-lying excited nuclear state of ^{129}Xe is induced. The experimental signature is a nuclear recoil observed together with the prompt deexcitation photon. We see no evidence for such inelastic WIMP-^{129}Xe interactions. A profile likelihood analysis allows us to set a 90% C.L. upper limit on the inelastic, spin-dependent WIMP-nucleon cross section of 3.3×10^{-38} cm^2 at 100 GeV/c^2. This is the most constraining result to date, and sets the pathway for an analysis of this interaction channel in upcoming, larger dual-phase xenon detectors.

DOI: 10.1103/PhysRevD.96.022008

I. INTRODUCTION

Astrophysical and cosmological evidence indicates that the dominant mass fraction of our Universe consists of some yet unknown form of dark or invisible matter. The dark matter could be made of stable or long-lived and yet undiscovered particles. Well-motivated theoretical models beyond the Standard Model of particle physics predict the existence of weakly interacting massive particles (WIMPs), which are natural candidates for dark matter. This hypothesis is currently being tested by several direct and indirect detection experiments, as well as at the LHC [1,2].

Most direct detection searches focus on elastic scattering of galactic dark matter particles off nuclei, where the keV-scale nuclear recoil energy is to be detected [3,4]. In this work, the alternative process of inelastic scattering is explored, where a WIMP-nucleus scattering induces a transition to a low-lying excited nuclear state. The experimental signature is a nuclear recoil detected together with the prompt deexcitation photon [5].

We consider the ^{129}Xe isotope, which has an abundance of 26.4% in natural xenon, and a lowest-lying $3/2^+$ state at 39.6 keV above the $1/2^+$ ground state. The electromagnetic nuclear decay has a half-life of 0.97 ns. The signatures and structure functions for inelastic scattering in xenon have been studied in detail in [6]. It was found that this channel, although not competitive in terms of sensitivity, is complementary to the spin-dependent, elastic scattering one, and that it dominates the integrated rates above $\simeq$10 keV of deposited energy. In addition, in the case of a positive signal, the observation of inelastic scattering would provide a clear indication of the spin-dependent nature of the fundamental interaction.

This paper is structured as follows. In Sec. II we briefly describe the main features of the XENON100 detector. In Sec. III we introduce the data sets employed in this analysis and detail the data analysis method, including the simulation of the expected signal and the background model. We conclude in Sec. IV with our results, and discuss the new constraints on inelastic WIMP-nucleus interactions.

II. THE XENON100 DETECTOR

The XENON100 experiment operates a dual-phase (liquid and gas) xenon time projection chamber (TPC) at the Laboratori Nazionali del Gran Sasso (LNGS) in Italy. It contains 161 kg of xenon in total, with 62 kg in the active region of the TPC. These are monitored by 178 1-inch square, low-radioactivity, UV-sensitive photomultiplier tubes (PMTs) arranged in two arrays, one in the liquid and one in the gas. The PMTs detect the prompt scintillation (S1) and the delayed, proportional scintillation signal (S2) created by a particle interacting in the active TPC region. The S2 signal is generated due to ionization electrons, drifted in an electric field of 530 V/cm and extracted into the gas phase by a stronger field of $\sim$12 kV/cm, where the proportional scintillation, or electroluminescence, takes place. The horizontal position, (x, y), of the interaction site is reconstructed from the position of the S2 shower, while the depth of the interaction, z, is given by the drift time measurement. The TPC thus yields a three-dimensional event localization, with an (x, y) resolution of $<$3 mm (1σ) and a z resolution of $<$0.3 mm (1σ), enabling us to reject the majority of background events via fiducial volume selections [7]. The ratio S2/S1 provides the basis for distinguishing between nuclear recoils (NRs), as induced by fast neutrons and expected from elastic WIMP-nucleus scatters, and electronic recoils (ERs) produced by β- and γ-rays. A 4 cm thick liquid xenon (LXe) layer surrounds the TPC and is monitored by 64 1-inch square PMTs, providing an effective active veto for further background reduction.

XENON100 has acquired science data between 2009 and 2015, and has set competitive constraints on spin-independent [8,9] and spin-dependent [9,10] elastic WIMP-nucleus scatters, on solar axions and galactic Axion Like Particles [11], as well as on leptophilic dark matter models [12–14].

Here we explore a new potential dark matter interaction channel in the XENON100 detector, caused by spin-dependent, inelastic WIMP-^{129}Xe interactions. The expected inelastic scattering signature is a combination between an ER and a NR, due to the short lifetime of the excited nuclear state and the short mean free path of $\sim$0.15 mm of the 39.6 keV deexcitation photon.

III. DATA ANALYSIS

This analysis is performed using XENON100 Run-II science data, with 224.6 live days of data taking. The detector's response to ERs has been characterized with

^{60}Co and ^{232}Th calibration sources, while the response to NRs was calibrated with an ^{241}AmBe (α, n)-source. The fast neutron from the latter gives rise to elastic and inelastic neutron-nucleus scatters, and can thus be employed to define the expected signal region for inelastic WIMP-nucleus scatters.

A. Signal correction

A particle interaction in the liquid xenon produces an S1 and a correlated S2 signal with a certain number of photoelectrons (PE) observed by the PMTs. The nonuniform scintillation light collection by the PMT arrays, due to solid angle effects, Rayleigh scattering length, reflectivity, transmission of the electrodes, etc., lead to a position-dependent S1 signal. The warping of the top meshes (inducing a variation in the width of the gas gap between the anode and the liquid-gas interface) and the absorption of electrons by residual impurities as they drift towards the gas region, as well as solid angle effects, lead to a position-dependent S2 signal. These signals are thus corrected in three dimensions, using various calibration data, as detailed in [7,15], with the corrected quantities denoted as cS1 and cS2, defined in [15].

B. Signal region and event selection

The inelastic scattering of a WIMP with a ^{129}Xe nucleus is expected to produce an energy deposit via a NR with the subsequent emission of a 39.6 keV deexcitation photon. The largest fraction of the energy released in the event is via the ER, due to the emitted photon which loses its energy in the LXe. This represents an unusual signature compared to the one expected from an elastic scatter, and makes the signal region overlap the ER background region. The region of interest (ROI) selected for this analysis surrounds the 39.6 keV xenon line in the (cS1,cS2)-plane and is based on ^{241}AmBe calibration data, where such inelastic scatters are induced by fast neutrons. The ROI extends from 60 to 210 PE in cS1, from 4×10^3 to 16×10^3 PE in cS2, such as to have at least 95% acceptance to all signal mass hypotheses. The ROI is further divided into subregions as shown in Fig. 1. These subregions were defined to contain a (roughly) similar number of expected background events in each region, where we cross-checked that changing the binning choice does not impact the sensitivity. The control regions (denoted as CR1 and CR2 in the figures), are selected to be as close as possible to the ROI, and are used for cross-checks of the background shape distribution.

Apart from the condition to occur in the defined ROI, valid events are required to fulfil several selection criteria, which can be summarized as follows: basic data quality cuts, energy selection and S2 threshold cut, veto cut for events with energy release in the detector's active LXe shield, selection of single-scatter events and of a predefined fiducial volume of 34 kg. Our analysis closely follows the event selection criteria described in detail in [15] for Run-II, with the following few exceptions. The cut on the width of the S2 signal as a function of drift time (where the maximal drift time is 176 μs and the width values range from ~1 to 2 μs) has been optimized on a sample of events selected from the 39.6 keV line and set to a 95% acceptance of these. This cut ensures that the broadening of S2 signals due to diffusion is consistent with the z-position calculated from the observed time difference between the S1 and S2 signals. Events are required to be single scatters by applying a threshold cut on the size of the second largest S2 peak. For this analysis, the threshold has been optimized to 160 PE and is constant with respect to the S2 signal size.

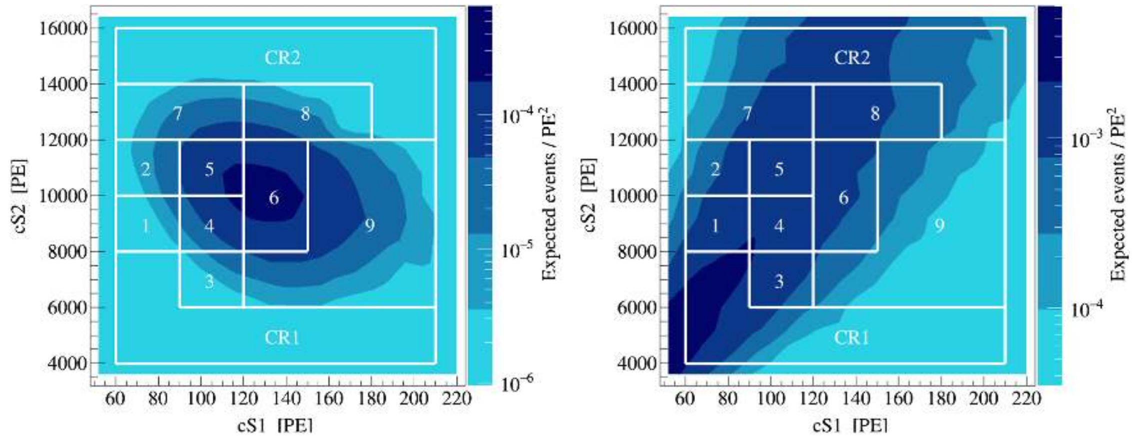

(a) (b)

FIG. 1. Signal (1–9) and control (CR1 and CR2) regions for the inelastic WIMP-^{129}Xe search in the (cS2,cS1)-plane. (a) shows the signal distribution for a simulated WIMP of mass 100 GeV/c^2 normalized to 50 events, while (b) is obtained using normalized ^{60}Co calibration data and represents the background expectation distribution.

C. Signal simulation

The detector response to inelastic WIMP-^{129}Xe interactions was simulated using an empirical signal model, described in this section. The total deposited energy is divided into two independent contributions: one coming from the 39.6 keV deexcitation photon and the other from the simultaneous nuclear recoil of the xenon atom. The detected light (S1) and charge (S2) signals are simulated separately for each of the two contributions and then added together. This recipe has been followed because the light and charge yields depend both on the type of interaction (ER vs NR) and on the deposited energy.

The distribution of an ER induced by the deexcitation photon in the (cS1,cS2)-plane is simulated assuming a two-dimensional normal probability distribution function (pdf), $f(\mathrm{cS1}_{\mathrm{er}}, \mathrm{cS2}_{\mathrm{er}})$, described (apart from a constant normalization factor) by the following equation:

$$\begin{aligned} f(\mathrm{cS1}_{\mathrm{er}}, \mathrm{cS2}_{\mathrm{er}}) &= \exp\left\{-\frac{1}{2(1-\rho^2)}\left[\frac{(\mathrm{cS1}_{\mathrm{er}}-\mu_{\mathrm{cS1}})^2}{\sigma_{\mathrm{cs1}}^2} + \frac{(\mathrm{cS2}_{\mathrm{er}}-\mu_{\mathrm{cS2}})^2}{\sigma_{\mathrm{cs2}}^2} \right.\right. \\ &\quad \left.\left. - \frac{2\rho\cdot(\mathrm{cS1}_{\mathrm{er}}-\mu_{\mathrm{cs1}})(\mathrm{cS2}_{\mathrm{er}}-\mu_{\mathrm{cs2}})}{\sigma_{\mathrm{cs1}}\sigma_{\mathrm{cs2}}}\right]\right\}, \end{aligned} \tag{1}$$

where μ_{cS1} and μ_{cS2} represent the average observed $\mathrm{cS1}_{\mathrm{er}}$ and $\mathrm{cS2}_{\mathrm{er}}$ signals given a 39.6 keV ER, σ_{cs1} and σ_{cs2} are the standard deviation in $\mathrm{cS1}_{\mathrm{er}}$ and $\mathrm{cS2}_{\mathrm{er}}$ respectively, and ρ stands for the correlation between the cS1 and cS2 signals. The detector-related light yield L_y at 39.6 keV, necessary to evaluate the average number of prompt photons detected (μ_{cS1}), is obtained from the NEST model [16–18] fit to data collected with several γ-lines. The same model is used to predict the charge yield at 39.6 keV, which is then scaled according to the detector's secondary scintillation gain Y. The latter is determined from the detector's response to single electrons [19]. The energy resolution at 39.6 keV in cS1 and cS2 has been measured to be 15.8% and 14.7%, respectively, and is used to extract the standard deviations σ_{cs1}, σ_{cs2}. The correlation parameter is measured using the 164 keV line from the decay of the ^{131m}Xe isomer ($T_{1/2} = 11.8$ d) produced during the ^{241}AmBe calibration. This γ-line is chosen since, unlike the 39.6 keV line, it is not associated with a NR and a measure of the (cS1,cS2) correlation of a pure ER interaction is possible. The correlation coefficient however depends on energy due to electron recombination effects. Its measured value at 164 keV is thus corrected based on the NEST expected recombination fractions for those energies. The corrected correlation coefficient is then $\rho = -0.4 \pm 0.1$.

The cS1 and cS2 distributions from the NR contribution are predicted starting from the expected nuclear recoil energy spectrum of WIMP inelastic interactions [6]. The average cS1 and cS2 are given by Eqs. (2) and (3) respectively:

$$\mathrm{cS1}_{\mathrm{nr}} = E_{\mathrm{nr}}\mathcal{L}_{\mathrm{eff}}(E_{\mathrm{nr}})L_y\frac{S_{\mathrm{nr}}}{S_{\mathrm{ee}}} \tag{2}$$

$$\mathrm{cS2}_{\mathrm{nr}} = E_{\mathrm{nr}}Q_Y(E_{\mathrm{nr}})Y, \tag{3}$$

where $\mathcal{L}_{\mathrm{eff}}$ is the liquid xenon scintillation efficiency for NRs relative to 122 keVee, while $S_{\mathrm{ee}} = 0.58$ and $S_{\mathrm{nr}} = 0.95$ describe the scintillation quenching due to the electric field of ER and NRs, respectively [20]. The parametrization and uncertainties of $\mathcal{L}_{\mathrm{eff}}$ as a function of nuclear recoil energy E_{nr} are based on existing direct measurements [21]. The light yield for 122 keV ERs is taken from the same NEST model fit as described above. For cS2, the parametrization of $Q_Y(E_{\mathrm{nr}})$ is taken from [22]. Finally, all detector-related resolution effects are introduced following the prescriptions described in [15].

The pdf's of the ER and NR contributions are then convolved to obtain the overall pdf of the expected signal. A 2D (cS1 versus cS2) acceptance map is applied to the signal pdf to reproduce data selection effects. Acceptances are computed separately for each selection criteria using the ^{241}AmBe calibration sample. Acceptances of other selections such as the liquid xenon veto cut, and the single-scatter interaction, represent an exception for which a dedicated computation has been performed. The combined acceptance of all selection criteria in the region of interest is roughly constant for all masses and averages to (0.80 ± 0.05). Figure 1(a) shows an example of a fully simulated signal model for a WIMP mass of 100 GeV/c^2, normalized to 50 events.

The described signal simulation was validated by reproducing the 39.6 keV xenon line activated from ^{241}AmBe neutrons and comparing it with data. For this purpose, the NR energy spectrum expected from inelastic neutron-^{129}Xe scatters has been obtained via Monte Carlo techniques, where we take into account the detector response and the nonuniform spatial distribution of events. The acceptance of our analysis selection criteria to this type of interaction have been recomputed. In particular, the acceptance to the double-scatter cut differs greatly between neutron and WIMPs scatters. Figure 2 shows a comparison between simulation (light blue) and calibration data (dark blue). Contour lines of equal densities are compared in Fig. 2(a), while Fig. 2(b) shows the cS1 projected distributions for different ranges in cS2.

D. Background model

The background in the region of interest for inelastic scattering is dominated by ERs and due to the residual radioactivity of detector materials, to ^{85}Kr present in the liquid xenon, and to ^{222}Rn decays in the liquid [23]. The background contribution from inelastic scatters of radiogenic or cosmogenic neutrons (producing a 39.6 keV deexcitation line) is negligible thanks to the very low expected neutron scattering rate in the detector [24].

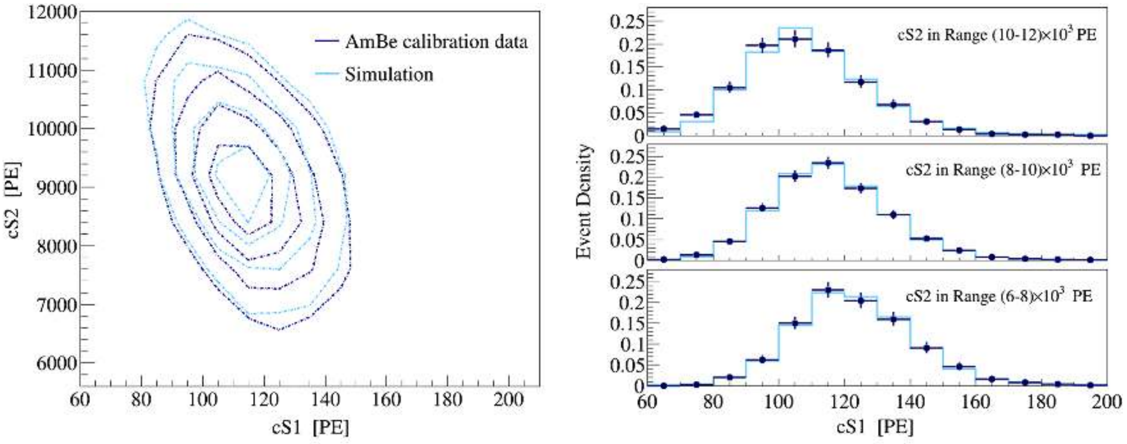

(a) (b)

FIG. 2. A full simulation (NR and ER response) of the 39.6 keV xenon line activated from ^{241}AmBe neutrons is compared with data. (a) compares contours of equal density in the (cS1,cS2)-plane, while (b) shows the same distribution projected in cS1 for several ranges of cS2. The histograms are normalized to unit area. Light and dark blue represent simulation and data, respectively.

The expected background is modeled using data from the ^{60}Co calibration campaign, which are assumed to represent well the background density distribution in the (cS1,cS2)-plane. The calibration sample yields about 2.2×10^4 events in the ROI; these are then scaled to the science data according to a measured scale factor $\tau_{\rm bkg}$. This scale factor, which is merely the ratio between the data and calibration sample yields, is measured in the two control regions shown in Fig. 1 (labeled CR1 and CR2) separately. The two control regions give compatible results and the computed average is $\tau_{\rm bkg} = 0.034 \pm 0.002$, where the reported uncertainty is of a statistical nature only.

The distribution of the calibration sample has been compared to the data of the science run in the two control regions, and agreement was found within statistical uncertainties. Furthermore, ^{60}Co calibration data have been compared in the region of interest to data from the ^{232}Th calibration campaign, and systematic uncertainties assessed based on it.

E. Systematic uncertainties

Uncertainties on the prediction of the total number of background events arise from the uncertainty on the measurement of the normalization factor, $\tau_{\rm bkg}$, and amount to 6%. Systematic uncertainty on the shape of the predicted background distribution is assessed by the maximal observed discrepancy in the ROI between the ^{60}Co and ^{232}Th calibration samples. The two samples' normalized yields are compared in each subregion and the overall largest deviation (incompatible with statistical fluctuation) is found to be within 4%. Consequently, a systematic uncertainty of 4% is assigned to the expected yield of each subregion. Uncertainties belonging to different subregions in the ROI are considered independent from one another.

Uncertainties on the total yield of signal events arising from selections are found to be only very weakly dependent on the WIMP mass, and an overall 6% acceptance uncertainty is applied to all WIMP hypotheses.

Uncertainties on the energy scale and, more generally, related to detector responses are parametrized using the respective uncertainties on the measures of L_y, $\mathcal{L}_{\rm eff}$, Y, Q_Y and ρ. The simulation shows that these uncertainties mainly affect the pdf of the signal model in the ROI, and very weakly the total signal yield. They are taken into account by simulating several signal pseudosamples for each WIMP mass, where the pseudosamples are produced by varying the model parameters by their ±1 standard deviation. For each subregion, an overall uncertainty is then computed by adding in quadrature the residual of each pseudosample with respect to the nominal. Figure 3 shows an example of such a systematic uncertainty computation for a WIMP mass of 100 GeV/c^2.

All the uncertainties discussed here are parametrized within a binned profile likelihood function using the ROOSTAT-ROOFIT framework [25,26]. All the parameters related to systematic uncertainties are assumed to be normally distributed.

IV. RESULTS AND DISCUSSION

This search is performed using XENON100 Run-II science data, which corresponds to an exposure of $34 \times 224.6\ \mathrm{kg} \cdot \mathrm{days}$. A total of 764 events are observed in the region of interest and no evidence of dark matter can be assessed based on an expected background of $756 \pm 5(\mathrm{stat}) \pm 55(\mathrm{syst})$ events. Figure 4 shows the distribution of events in the region of interest, where the bottom panel displays the ratio between data and expected background. The light and dark blue shaded areas represent the statistical and systematic uncertainty on the background

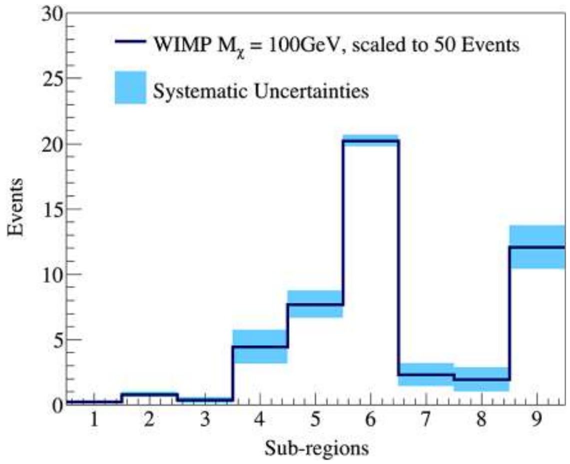

FIG. 3. Predicted signal yield in each subregion (blue curve), along with systematic uncertainties (shaded area) simulated for a WIMP mass of 100 GeV/c^2. The signal has been scaled for a total number of 50 events. The subregions are defined in Fig. 1.

expectation, respectively. The expected signal for a WIMP mass of 100 GeV/c^2, normalized to a total of 50 events, is also shown.

This result is interpreted via a binned profiled likelihood approach by means of the test statistic $\tilde{q}$ and its asymptotic distributions, as described in [27]. Assuming an isothermal WIMP halo with a local density of $\rho_\chi = 0.3$ GeV/cm^3, a local circular velocity of $v_0 = 220$ km/s, a galactic escape velocity of $v_{\mathrm{esc}} = 544$ km/s [28] and the nuclear structure factors as computed in [6], a 90% CL$_s$ [29] confidence level upper limit is set on the spin-dependent inelastic WIMP-nucleon cross section as a function of the WIMP mass. The CL$_s$ technique helps to protect against excluding a cross section which is smaller than the experimental sensitivity.

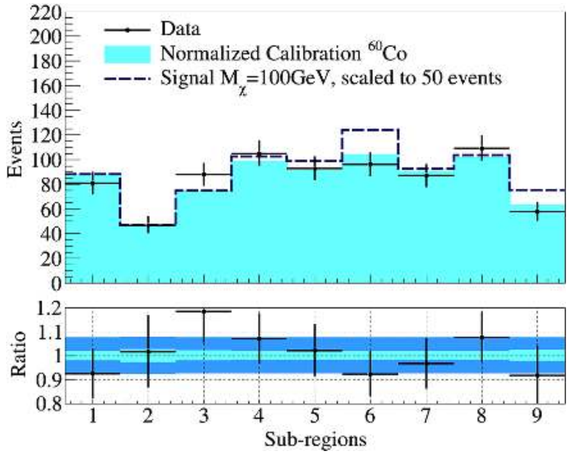

FIG. 4. Distribution of observed events in the region of interest (data points), along with the normalized distribution from calibration data (filled histogram). The expected signal for a WIMP mass of 100 GeV/c^2 (blue dashed), normalized to a total of 50 events, is also shown. The bottom panel displays the ratio between data and expected background, where the light and dark blue shaded areas represent the statistical and systematic uncertainty on the background expectation, respectively.

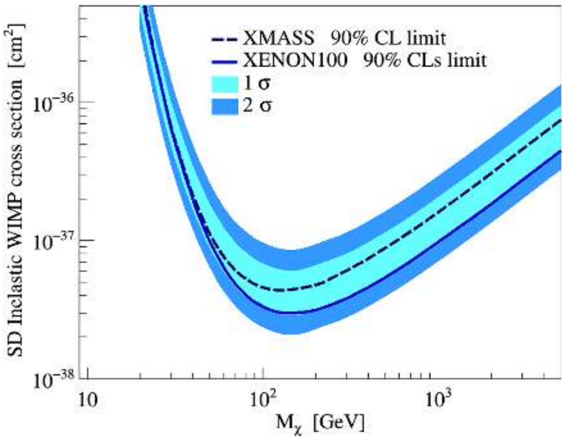

FIG. 5. Upper limit (blue curve) on the spin-dependent, inelastic WIMP-nucleon cross section as a function of WIMP mass. The expected one (light shaded area) and two (dark shaded area) standard deviation uncertainties are also shown. This result is compared to the upper limit (at 90% C.L.) obtained by the XMASS experiment (dashed line) [30].

Our result is shown in Fig. 5, together with its expected one and two sigma statistical variation. The most constraining limit is set for a WIMP of mass 100 GeV/c^2 to a cross section of 3.3×10^{-38} cm^2 (at 90% CL$_s$ confidence level).

This result is compared to the one obtained by the XMASS experiment [30], a single-phase liquid xenon detector, which used a fiducial volume containing 41 kg of LXe and 165.9 live days of data.

While these upper limits are not competitive to spin-dependent, elastic scattering results, as obtained by XENON100 [10] and LUX [31] (bounding the cross section to be $<1 \times 10^{-40}$ cm^2, at 90% C.L., for a 100 GeV/c^2 WIMP), our results are the most stringent for the spin-dependent inelastic channel, and set the stage for a sensitive search of inelastic WIMP-nucleus scattering in running or upcoming liquid xenon experiments such as XENON1T [32], XENONnT [32], LZ [33], and DARWIN [34]. In these larger detectors, with lower intrinsic backgrounds from ^{85}Kr and ^{222}Rn decays, and improved self-shielding, the electronic recoil background will be reduced by a few orders of magnitude with respect to XENON100, and ultimately limited by solar neutrino interactions [35]. The discovery of this interaction channel would be a clear signature for a spin-dependent nature of the dark matter interaction, and would provide a potential handle to constrain the WIMP mass with data from one experiment only [6,36].

ACKNOWLEDGMENTS

We gratefully acknowledge support from the National Science Foundation, Swiss National Science Foundation, Deutsche Forschungsgemeinschaft, Max Planck Gesellschaft, German Ministry for Education and Research, Netherlands Organisation for Scientific Research, Weizmann Institute of Science, I-CORE, Initial Training Network Invisibles (Marie Curie Actions, PITNGA-2011-289442), Fundacao para a Ciencia e a Tecnologia, Region des Pays de la Loire, Knut and Alice Wallenberg Foundation, Kavli Foundation, and Istituto Nazionale di Fisica Nucleare. We are grateful to Laboratori Nazionali del Gran Sasso for hosting and supporting the XENON project.

---

[1] J. Silk *et al.*, *Particle Dark Matter: Observations, Models and Searches*, edited by G. Bertone (Cambridge Univ. Press, Cambridge, 2010).

[2] L. Baudis, Dark matter detection, J. Phys. G **43**, 044001 (2016).

[3] T. Marrodan Undagoitia and L. Rauch, Dark matter direct-detection experiments, J. Phys. G **43**, 013001 (2016).

[4] L. Baudis, Dark matter searches, Ann. Phys. (Berlin) **528**, 74 (2016).

[5] John R. Ellis, R. A. Flores, and J. D. Lewin, Rates for inelastic nuclear excitation by dark matter particles, Phys. Lett. B **212**, 375 (1988).

[6] L. Baudis, G. Kessler, P. Klos, R. F. Lang, J. Menéndez, S. Reichard, and A. Schwenk, Signatures of dark matter scattering inelastically off nuclei, Phys. Rev. D **88**, 115014 (2013).

[7] E. Aprile *et al.* (XENON100 Collaboration), The XENON100 dark matter experiment, Astropart. Phys. **35**, 573 (2012).

[8] E. Aprile *et al.* (XENON100 Collaboration), Dark Matter Results from 225 Live Days of XENON100 Data, Phys. Rev. Lett. **109**, 181301 (2012).

[9] E. Aprile *et al.* (XENON100 Collaboration), XENON100 dark matter results from a combination of 477 live days, Phys. Rev. D **94**, 122001 (2016).

[10] E. Aprile *et al.* (XENON100 Collaboration), Limits on Spin-Dependent WIMP-Nucleon Cross Sections from 225 Live Days of XENON100 Data, Phys. Rev. Lett. **111**, 021301 (2013).

[11] E. Aprile *et al.* (XENON100 Collaboration), First axion results from the XENON100 experiment, Phys. Rev. D **90**, 062009 (2014).

[12] E. Aprile *et al.* (XENON100 Collaboration), Exclusion of leptophilic dark matter models using XENON100 electronic recoil data, Science **349**, 851 (2015).

[13] E. Aprile *et al.* (XENON100 Collaboration), Search for Event Rate Modulation in XENON100 Electronic Recoil Data, Phys. Rev. Lett. **115**, 091302 (2015).

[14] E. Aprile *et al.* (XENON Collaboration), Search for Electronic Recoil Event Rate Modulation with 4 Years of XENON100 Data, Phys. Rev. Lett. **118**, 101101 (2017).

[15] E. Aprile *et al.* (XENON100 Collaboration), Analysis of the XENON100 dark matter search data, Astropart. Phys. **54**, 11 (2014).

[16] M. Szydagis, A. Fyhrie, D. Thorngren, and M. Tripathi, Enhancement of NEST capabilities for simulating low-energy recoils in liquid xenon, J. Instrum. **8**, C10003 (2013).

[17] J. Allison *et al.*, Geant4 developments and applications, IEEE Trans. Nucl. Sci. **53**, 270 (2006).

[18] S. Agostinelli *et al.* (GEANT4 Collaboration), GEANT4: A simulation toolkit, Nucl. Instrum. Methods Phys. Res., Sect. A **506**, 250 (2003).

[19] E. Aprile *et al.*, Observation and applications of single-electron charge signals in the XENON100 experiment, J. Phys. G **41**, 035201 (2014).

[20] E. Aprile, C. E. Dahl, L. de Viveiros, R. J. Gaitskell, K. L. Giboni, J. Kwong, P. Majewski, K. Ni, T. Shutt, and M. Yamashita, Simultaneous Measurement of Ionization and Scintillation from Nuclear Recoils in Liquid Xenon as Target for a Dark Matter Experiment, Phys. Rev. Lett. **97**, 081302 (2006).

[21] E. Aprile *et al.* (XENON100 Collaboration), Dark Matter Results from 100 Live Days of XENON100 Data, Phys. Rev. Lett. **107**, 131302 (2011).

[22] E. Aprile *et al.* (XENON100 Collaboration), Response of the XENON100 dark matter detector to nuclear recoils, Phys. Rev. D **88**, 012006 (2013).

[23] E. Aprile *et al.* (XENON100 Collaboration), Study of the electromagnetic background in the XENON100 experiment, Phys. Rev. D **83**, 082001 (2011); Erratum, Phys. Rev. D **85**, 029904(E) (2012).

[24] E. Aprile *et al.* (XENON100 Collaboration), The neutron background of the XENON100 dark matter search experiment, J. Phys. G **40**, 115201 (2013).

[25] L. Moneta *et al.*, *Proc. Sci.*, ACAT2010 (2010) 057.

[26] W. Verkerke and D. P. Kirkby, *Statistical Problems in Particle Physics, Astrophysics and Cosmology (PHYSTAT 05): Proceedings, Oxford, UK, 2005*, eConf C0303241, MOLT007 (2003).

[27] G. Cowan, K. Cranmer, E. Gross, and O. Vitells, Asymptotic formulae for likelihood-based tests of new physics, Eur. Phys. J. C **71**, 1554 (2011); Erratum, Eur. Phys. J. C **73**, 2501(E) (2013).

[28] M. C. Smith *et al.*, The RAVE survey: Constraining the local galactic escape speed, Mon. Not. R. Astron. Soc. **379**, 755 (2007).

[29] A. L. Read, Modified frequentist analysis of search results (The CL(s) method), in *Workshop on confidence limits, CERN, Geneva, Switzerland, 2000: Proceedings* (2000), pp. 81–101, http://weblib.cern.ch/abstract?CERN-OPEN-2000-205.

[30] H. Uchida *et al.* (XMASS-I Collaboration), Search for inelastic WIMP nucleus scattering on ^{129}Xe in data from the XMASS-I experiment, Prog. Theor. Exp. Phys. **2014**, 63C01 (2014).

[31] D. S. Akerib *et al.* (LUX Collaboration), Results on the Spin-Dependent Scattering of Weakly Interacting Massive Particles on Nucleons from the Run 3 Data of the LUX Experiment, Phys. Rev. Lett. **116**, 161302 (2016).

[32] E. Aprile *et al.* (XENON Collaboration), Physics reach of the XENON1T dark matter experiment, J. Cosmol. Astropart. Phys. 04 (2016) 027.

[33] D. S. Akerib *et al.* (LZ Collaboration), LUX-ZEPLIN (LZ) conceptual design report, arXiv:1509.02910.

[34] J. Aalbers *et al.* (DARWINLZ Collaboration), DARWIN: Towards the ultimate dark matter detector, J. Cosmol. Astropart. Phys. 11 (2016) 017.

[35] L. Baudis, A. Ferella, A. Kish, A. Manalaysay, T. M. Undagoitia, and M. Schumann, Neutrino physics with multi-ton scale liquid xenon detectors, J. Cosmol. Astropart. Phys. 01 (2014) 044.

[36] C. McCabe, Prospects for dark matter detection with inelastic transitions of xenon, J. Cosmol. Astropart. Phys. 05 (2016) 033.